Annals of Biomedical Engineering, Vol. 30, pp. 555–565, 2002
Printed in the USA. All rights reserved.

0090-6964/2002/30(4)/555/11/$15.00

Modeling of Nonlinear Physiological Systems with Fast and Slow Dynamics. II. Application to Cerebral Autoregulation

G. D. MITSIS,[1] R. ZHANG,[2] B. D. LEVINE,[2] and V. Z. MARMARELIS[1]

[1]Department of Biomedical Engineering, University of Southern California, Los Angeles, CA and [2]Institute for Exercise and Environmental Medicine, University of Texas Southwestern Medical Center at Dallas and Presbyterian Hospital of Dallas, Dallas, TX

(Received 30 April 2001; accepted 24 January 2002)

Abstract—Dynamic autoregulation of cerebral hemodynamics in healthy humans is studied using the novel methodology of the Laguerre–Volterra network for systems with fast and slow dynamics (Mitsis, G. D., and V. Z. Marmarelis, *Ann. Biomed. Eng.* 30:272–281, 2002). Since cerebral autoregulation is mediated by various physiological mechanisms with significantly different time constants, it is used to demonstrate the efficacy of the new method. Results are presented in the time and frequency domains and reveal that cerebral autoregulation is a nonlinear and dynamic (frequency-dependent) system with considerable nonstationarities. Quantification of the latter reveals greater variability in specific frequency bands for each subject in the low and middle frequency range (below 0.1 Hz). The nonlinear dynamics are prominent also in the low and middle frequency ranges, where the frequency response of the system exhibits reduced gain. *© 2002 Biomedical Engineering Society.* [DOI: 10.1114/1.1477448]

Keywords—Cerebral autoregulation, Cerebral hemodynamics, Nonlinear modeling, Nonstationary systems, Volterra kernels, Lagurre–Volterra network.

INTRODUCTION

The traditional concept of cerebral autoregulation refers to the ability of the cerebrovascular bed to maintain a relatively constant steady-state cerebral blood flow despite changes in steady-state cerebral perfusion pressure.[7,16] Intact cerebral autoregulation is very important, because of the high aerobic metabolic rate of cerebral tissue (around 15% of the cardiac output is received by the brain under resting conditions). Even a short interruption in cerebral blood flow may result in loss of consciousness.[7,16] Under normal conditions, it has been observed that a sudden drop in the pressure level causes an initial change in the level of blood flow that gradually returns to its previous value within a couple of minutes, due to multiple homeostatic regulatory mechanisms that control cerebrovascular resistance.[7,16]

Address correspondence to Professor V. Z. Marmarelis, OHE 500, USC, Los Angeles, CA 90089-1451. Electronic mail: vzm@bmsrs.usc.edu

This has led to the view of cerebral autoregulation as a static phenomenon, whereby the steady-state pressure-flow relationship is described by a sigmoidal curve with a wide plateau, suggesting that cerebral blood flow remains constant despite changes in pressure. However, this description reveals no information about the dynamic properties of cerebral autoregulation and the quantitative manner in which rapid changes in pressure induce rapid changes in flow.

With the development of transcranial Doppler (TCD) ultrasonography for the noninvasive measurement of cerebral blood flow velocity in the middle cerebral artery with high temporal resolution, it has been shown that blood flow velocity can vary rapidly in response to variations of systemic arterial blood pressure over various time scales.[11,20] We will consider data representing the mean arterial blood pressure (ABP) and mean cerebral blood flow velocity (CBFV), computed as averages over each heart beat interval (marked by the $R-R$ peaks in the ECG), and resampled evenly every second (see Methods).

The availability of such high temporal resolution data offers the opportunity to study dynamic cerebral autoregulation in humans, using recently developed nonlinear modeling methods.[12] In addition to conventional experiments, such as rapid deflation of thigh pressure cuffs,[1,19] Valsalva maneuvers,[18] or forced breathing maneuvers,[4] spontaneous fluctuations in beat-to-beat ABP and CBFV data possess broadband spectral properties and have been used for the study of both cerebral[6,8,13,15,21] and renal[2,3] autoregulation using linear[6,8,13,21] and nonlinear[2,3,15] modeling methods. Impulse response and transfer function analysis were utilized to show that cerebral autoregulation is more effective in the low-frequency range (below 0.1 Hz), where most of the ABP spectral power resides (i.e., most spontaneous ABP changes do not cause large CBFV variations). These studies have also indicated the presence of significant nonlinearities in this low-frequency range by means of coherence function measurements,[21] suggesting that cerebral autoregulation

mechanisms exhibit dynamic (i.e., frequency dependent) nonlinearities. This presents the motivation for the present study.

The goal of this study is to examine the nonlinear dynamic relationship between beat-to-beat changes in ABP and CBFV, which reflects the combined effect of multiple mechanisms of cerebral autoregulation. Since the cerebrovascular bed is controlled by metabolic, myogenic, endothelium-related, and neural mechanisms[5,15,16] the dynamics of cerebral autoregulation are active over widely different frequency bands (from 0.005 to 0.5 Hz). For example, metabolic mechanisms may be more active at very low frequencies and myogenic mechanisms may be active at high frequencies, while endothelium-related and autonomic activity may be found in the intermediate frequency bands.[21]

For this reason, it is incumbent on the employed modeling methodology to be able to capture reliably both fast and slow dynamics in a single processing task. To this purpose, we employ a recently developed nonlinear modeling method, based on a variant of the general Volterra–Wiener approach, that utilizes the Laguerre–Volterra network (LVN) with two filter banks to model nonlinear systems with fast and slow dynamics effectively.[12] Note that a recently published study on nonlinear modeling of cerebral autoregulation,[15] using the Laguerre expansion of Volterra kernels technique,[10] seems to have captured only the fast system dynamics (at frequencies higher than 0.1 Hz).

In the present paper, an accurate nonlinear model that includes important low-frequency autoregulation dynamics is obtained using this novel methodology, and showcases its application to physiological systems with fast and slow dynamics.

EXPERIMENTAL METHODS

Five healthy subjects (four male and one female, age: 30 ± 9 years, weight: 77 ± 16 kg, height: 176 ± 8 cm) voluntarily participated in the study. All the subjects were nonsmokers and free of any known cardiovascular, pulmonary, or cerebrovascular diseases. The subjects had been informed about the experimental procedures and each one signed a written consent form approved by the Institutional Review Boards of the University of Texas Southwestern Medical Center and the Presbyterian Hospital of Dallas. The experiments were conducted postprandial after 2 h in an environmentally controlled laboratory with an ambient temperature of 25 °C. The subjects were refrained from heavy exercise, caffeinated or alcohol beverages for at least 24 h before the experiments. After about 30 min of supine rest, arterial pressure and blood flow velocity were recorded continuously for a period of about 2 h.

Arterial pressure was measured in the finger by photoplethysmography (Finapres, Ohmeda). The measurements were obtained from the two middle fingers alternatively (every 20 min) to prevent discomfort of the subject and also to prevent prolonged recordings from one finger from affecting the accuracy of the measurements. The data segments collected from each finger were processed off-line to construct a continuous time series of arterial pressure, as detailed in Ref. 21. The reliability and accuracy of the finger pressure measurements was corroborated with intermittent pressure measurements at the brachial artery by using electrosphygmomanometry (Suntech).

Cerebral blood flow velocity was measured in the middle cerebral artery by using TCD. A 2 MHz Doppler probe (Multiflow, DWL Elektronische Systeme) was placed over the temporal window and was fixed at a constant angle and position with adjustable head gear to obtain optimal signals. The ultrasound transducer power was constant (ranging from 50 to 60 mW/cm^2) during the recordings. The power level was adjusted to obtain an optimal signal, while at the same time being kept as low as possible, below the safety limits recommended by the American Institute for Ultrasound in Medicine and Biology. End-tidal CO_2 was monitored continuously with a nasal cannula using a mass spectrometer (MGA 1100, Marquette Electronics).

The analog signals of ABP and CBFV were sampled simultaneously at 100 Hz and were digitized at 12 bits (Multi-Dop X2, DWL). Real time beat-to-beat mean values of ABP and CBFV were calculated by integrating the waveform of the sampled signals within each cardiac cycle ($R-R$ interval). The beat-to-beat values were then linearly interpolated and resampled at 1 Hz (after antialiasing low-pass filtering) to obtain equally spaced time series of ABP and CBFV data for the subsequent analysis.

MATHEMATICAL METHODS

The modeling of the dynamic nonlinearities present in cerebral autoregulation is performed with a novel variant of the general Volterra–Wiener approach that utilizes the LVN with two filter banks, shown in Fig. 1 and discussed in detail in the companion paper.[12] Some of its basic features are highlighted below.

The free parameters of the LVN are the Laguerre parameters (a_1, a_2) of the two filter banks $\{b_j^{(1)}\}$ and $\{b_j^{(2)}\}$, the connection weights $\{w_{k,j}^{(i)}\}$, the polynomial coefficients $\{c_{m,k}\}$ and the output offset y_0. Their total number is equal to $(L_1+L_2+2+Q)K+1$, where (L_1, L_2) are the maximum orders of the Laguerre functions employed in the two filter banks, Q is the order of the polynomial activation functions, and K is the number of hidden units.

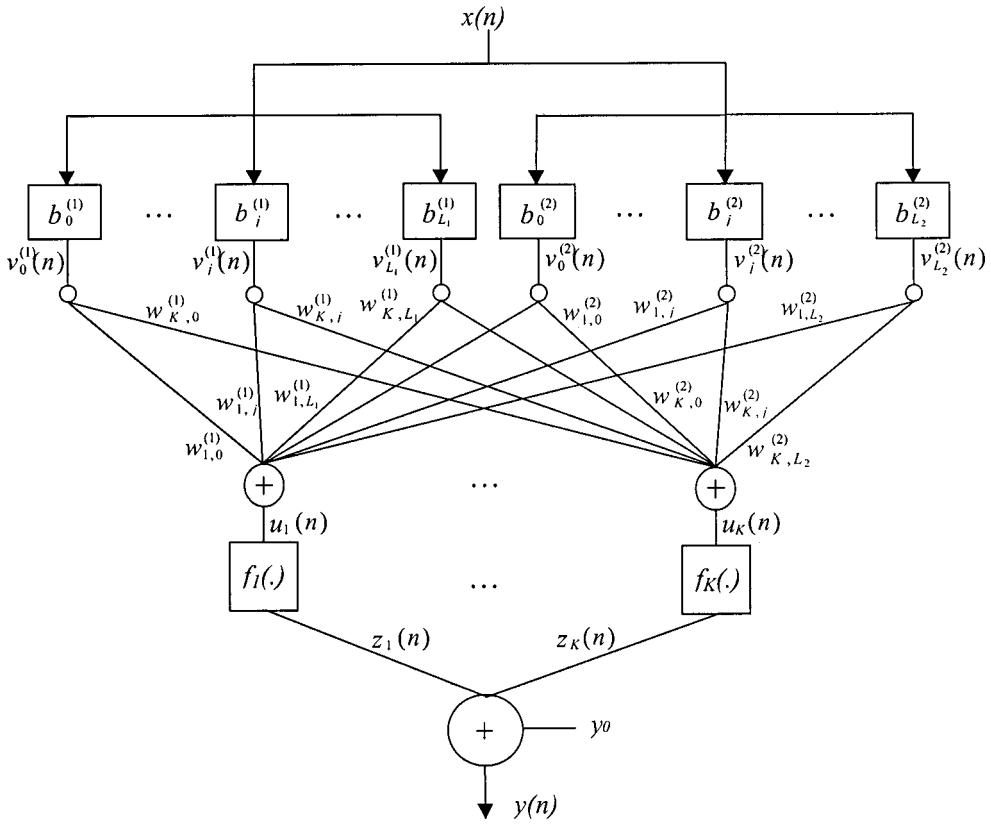

FIGURE 1. The Laguerre–Volterra network with two filter banks. In the figure, n denotes discrete time, $x(n)$ is the input signal, $b_j^{(i)}(n)$ and $v_j^{(i)}(n)$ are the jth order discrete-time Laguerre function and the output of the jth Laguerre filter of the ith filter bank, respectively, $w_{k,j_i}^{(i)}$ is the connection weight between the kth hidden unit and the jth order filter of the ith filter bank, $u_k(n)$ is the input of the kth hidden unit, given by $u_k(n)=\Sigma_{i=1}^{2}\Sigma_{j=0}^{L_i} w_{k,j}^{(i)} v_j^{(i)}(n)$, $z_k(n)$ is the corresponding hidden unit output, given by $z_k(n)=f_k[u_k(n)]=\Sigma_{m=1}^{Q} c_{m,k} u_k^m(n)$, and $y(n)$ is the network output, given by $y(n)=\Sigma_{k=1}^{K} z_k(n)+y_0$.

The LVN with two filter banks can yield accurate nonlinear models from short input-output data records, by using the latter to train the network parameters via the error backpropagation algorithm. This is done through the following iterative relations:

$$w_{k,j_i}^{(i),(r+1)} = w_{k,j_i}^{(i),(r)} + \gamma_w \lfloor \epsilon(n) f_k'[u_k(n)] v_{j_i}^{(i)}(n) \rfloor_r, \quad (1)$$

$$c_{m,k}^{(r+1)} = c_{m,k}^{(r)} + \gamma_C \lfloor \epsilon(n) u_k^m(n) \rfloor_r, \quad (2)$$

$$y_0^{(r+1)} = y_0^{(r)} + \gamma_y [\epsilon(n)]_r, \quad (3)$$

$$a_i^{(r+1)} = a_i^{(r)} + \gamma_i \sum_{k=1}^{K} \sum_{m=0}^{Q} \sum_{j=0}^{L_i} m \left[c_{m,k} w_{k,j}^{(i)} \epsilon(n) \times u_k^{m-1}(n) \frac{\partial v_j^{(i)}(n)}{\partial a_i} \right]_r, \quad (4)$$

where the network variables and parameters are defined in Fig. 1, $\epsilon(n)$ is the output prediction error, f_k' denotes the derivative of f_k with respect to u_k, r denotes the iteration index and $\gamma_w, \gamma_c, \gamma_y, \gamma_i$ are fixed positive learning constants. Note that the variables $v_j^{(i)}(n)$, $u_k(n)$, $f_k''(n)$, and $\epsilon(n)$ are evaluated at the rth iteration in Eqs. (1)–(4).

With the use of two Laguerre filter banks characterized by distinct Laguerre parameters (a_1, a_2) we can model the fast and slow dynamics of a nonlinear system separately (as in the case of cerebral autoregulation) in a single processing task. The LVN representation of a system is equivalent to the general Volterra model (shown below for a Qth order system):

$$y(n) = \sum_{n=0}^{Q} \left[\sum_{m1=0}^{M} \cdots \sum_{m_n=0}^{M} k_n(m_1,..,m_n) x(n-m_1) \cdots x(n-m_n) \right], \quad (5)$$

where $x(n)$ is the system input, $y(n)$ is the system output, M is the system memory, and $k_n(m_1,\ldots,m_n)$ is the

*n*th order Volterra kernel describing the *n*th order (linear and nonlinear) dynamics of the system. The Volterra kernels in Eq. (5) can be expressed in terms of the trained network parameters as

$$k_0 = y_0, \tag{6}$$

$$k_1(m_1) = \sum_{k=1}^{K} c_{1,k} \sum_{i=1}^{2} \sum_{j=0}^{L_i} w_{k,j}^{(i)} b_j^{(i)}(m_1), \tag{7}$$

$$k_2(m_1, m_2) = \sum_{k=1}^{K} c_{2,k} \sum_{i_1=1}^{2} \sum_{i_2=1}^{2} \sum_{j_1=0}^{L_{i_1}} \sum_{j_2=0}^{L_{i_2}} w_{k,j_1}^{(i_1)} \times w_{k,j_2}^{(i_2)} b_{j_1}^{(i_1)}(m_1) b_{j_2}^{(i_2)}(m_2), \tag{8}$$

$$k_n(m_1, \ldots, m_n) = \sum_{k=1}^{K} c_{n,k} \sum_{i_1=1}^{2} \cdots \sum_{i_n=1}^{2} \sum_{j_1=0}^{L_{i_1}} \cdots \sum_{j_n=0}^{L_{i_n}} w_{k,j_1}^{(i_1)} \ldots w_{k,j_n}^{(i_n)} b_{j_1}^{(i_1)}(m_1) \ldots b_{j_n}^{(i_n)}(m_n), \tag{9}$$

therefore they can be obtained after the training (estimation) of the network parameters using the input-output data.

The input signal is the ABP data and the output signal is the CBFV data, described in Experimental Methods. 6 min data segments (which correspond to 360 data points) are employed in the training procedure, after high-pass filtering at 0.005 Hz to remove very slow trends in the data.

The structural parameters of the LVN are selected by considering the normalized mean-square error (NMSE) of the output prediction achieved by the model for the training data, defined as the sum of the squares of the errors between the model prediction and the true output over the sum of the squares of the true output, using the "minimum description length" (MDL) criterion.[17] This ensures that we obtain an accurate representation of the system and avoid overfitting the model to the specific data segment. Following this procedure, a LVN with $L_1 = L_2 = 7$, $K = 3$, and $Q = 2$ is selected in all cases. Note that the total number of unknown parameters in this model is 55, which is extremely low compared to the conventional cross-correlation technique,[9] which would require the estimation of over 5150 values for the first- and second-order kernels with the necessary memory of 100 lags. The achieved model parsimony is accompanied by a significant improvement in the prediction NMSE relative to the conventional cross-correlation technique. In order to terminate the training procedure and avoid overtraining the network, the prediction NMSE is minimized for a 2 min forward segment of testing data (adjacent to the 6 min training data segment).

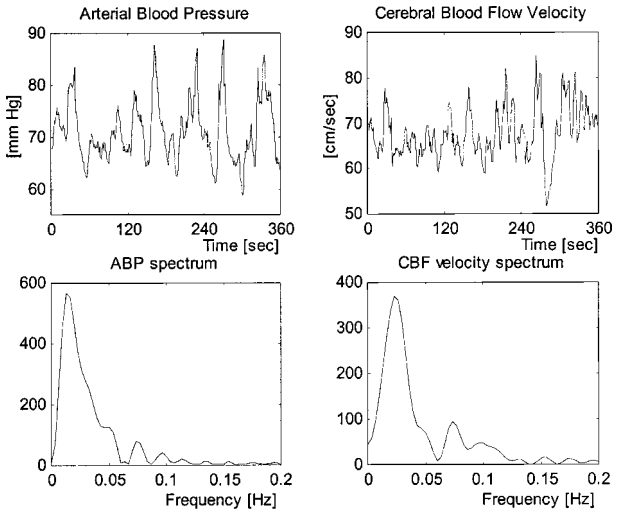

FIGURE 2. Typical ABP and CBFV data used for model estimation. Top panels: time series, bottom panels: spectra after high-pass filtering at 0.005 Hz.

The utility of using two filter banks versus one filter bank is demonstrated by comparing the out-of-sample NMSEs (for the testing data) of the two networks for the same number of free parameters. Specifically, the analysis was repeated for a one filter bank LVN with $L = 15$, $K = 3$, and $Q = 2$, and the results are given in the next section.

RESULTS

The averages of the ABP and CBFV data over the 2 h recordings from each of the five subjects are 82.3 ± 10.7 mm Hg and 61.7 ± 9.0 cm/s respectively. Typical 6 min segments of ABP and CBFV data are shown in Fig. 2, along with their corresponding spectra. Most of the signal power lies below 0.10 Hz, and negligible power lies above 0.2 Hz (the average respiratory frequency). The average achieved (in-sample) output prediction NMSEs using first- and second-order LVN models are $49.1\% \pm 13.4\%$ and $27.6\% \pm 9.5\%$, respectively. The reduction of the prediction NMSE from the first-order (linear) model to the second-order (nonlinear) model is significant (over 20%) and satisfies the MDL criterion used for model order determination (see Methods), confirming the fact that dynamic cerebral autoregulation is nonlinear. The NMSE reduction from the second-order to the third-order LVN model does not meet the MDL criterion and a second-order model is selected.

The performance of the LVN modeling approach is illustrated in Fig. 3, where we show the actual CBFV output (top trace) along with the obtained LVN model prediction (second trace), as well as its first- and second-order components (third and fourth traces, respectively).

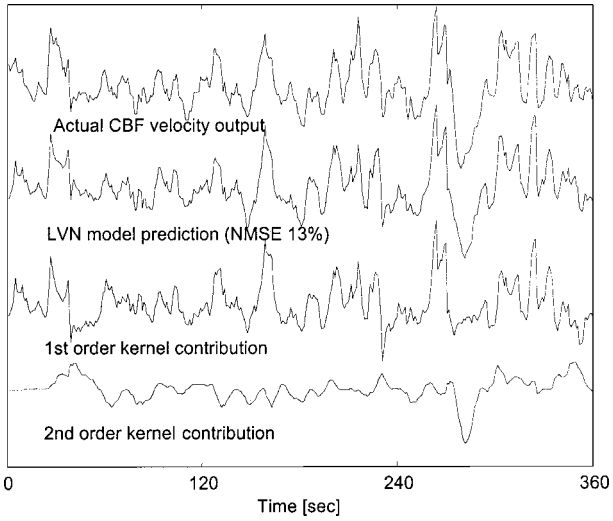

FIGURE 3. Typical LVN model prediction.

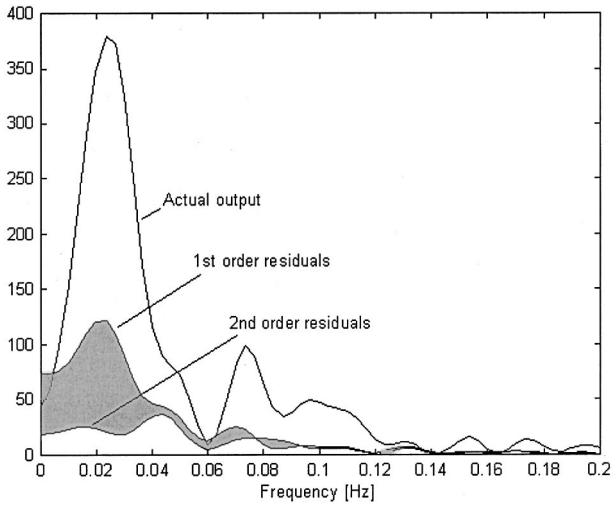

FIGURE 4. Spectra of the output (CBFV), first-, and second-order model residuals. The shaded area shows the effect of the nonlinear term in the frequency domain.

For this specific data segment, the prediction NMSE is 13%, and the first-order (linear) prediction NMSE is 34% (i.e., the NMSE reduction due to the second-order kernel is 21%). We must note that the contribution of the second-order kernel (nonlinear term) to the output prediction NMSE demonstrated considerable variability among data segments (as small as 8% and as large as 62%). This variability was also reflected in the form of the second-order kernel estimates among different segments and/or subjects. This finding may suggest either nonstationary behavior in the nonlinearity of the system or the intermodulatory (nonlinear) influence of other exogenous variables (e.g., changes in arterial CO_2).

The relative contributions of the linear and nonlinear terms of the model are also illustrated in Fig. 4 for the same set of data in the frequency domain, where the output spectrum and the spectra of the first-order and second-order residuals (output prediction errors) are shown. The shaded area corresponds to the difference between the first- and second-order model residuals in the frequency domain, indicating that the nonlinearities are found below 0.1 Hz and are prominent below 0.04 Hz. This observation is consistent throughout all the data segments, and agrees with previous findings based on the estimated coherence function.[21]

A typical estimated first-order kernel, which describes the linear dynamics of the system, is shown in Fig. 5 in the time domain using logarithmic time scale (the lag values are incremented by one for this purpose). The decomposition of the kernel into a fast and a slow component is performed by the two filter banks of the LVN and is shown on the left panel of Fig. 5, whereas the total first-order kernel is shown in the right panel. Note the large positive value at zero lag and the significant negative values between 1 and 5 s (lags). Smaller values extend up to about 150 s. In this case, the fast component corresponds to a Laguerre parameter of 0.19, while the slow component corresponds to a Laguerre parameter of 0.76. The averaged values for the two Laguerre parameters over the five subjects are 0.24 ± 0.04 and 0.79 ± 0.05, respectively.

The fast Fourier transform (FFT) magnitudes of the first-order kernel and its two components are shown in Fig. 6 in log–log scale. The fast component has a high-pass (differentiating) characteristic with a peak around 0.2 Hz and a ''shoulder'' around 0.075 Hz, while the slow component exhibits a peak around 0.025 Hz and a trough around 0.01 Hz. The total first-order frequency response (i.e., the FFT magnitude of the first-order ker-

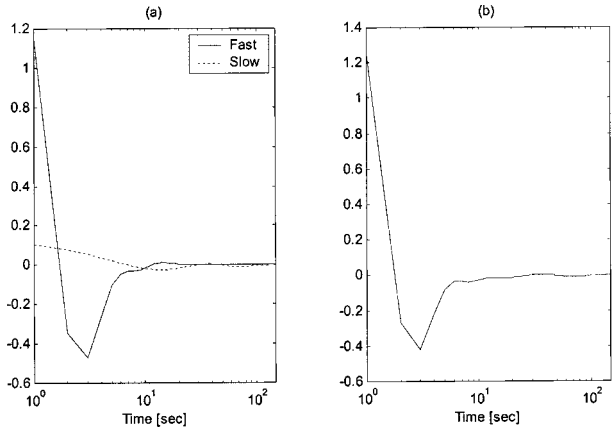

FIGURE 5. Typical first-order kernel in logarithmic time scale: (a) Solid line: fast component, dotted line: slow components and (b) total kernel. Note that the time lag values are incremented by 1 to make the logarithmic scale at zero lag possible.

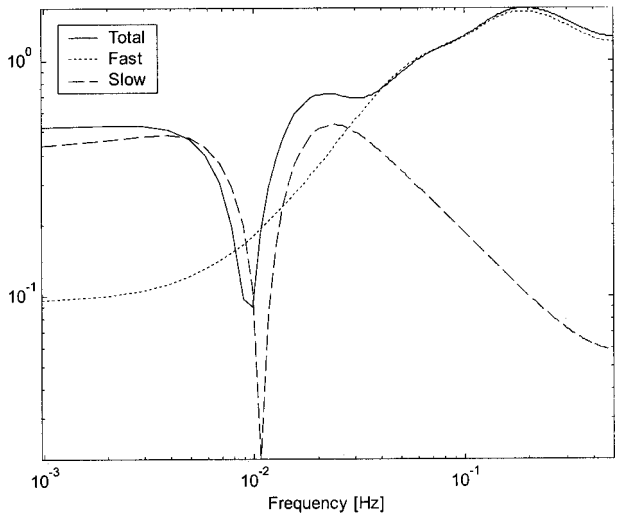

FIGURE 6. FFT magnitude of the first-order kernel (linear frequency response function) and its components shown in Fig. 5. Solid line: total, dotted line: fast component, dashed line: slow component.

nel) is dominated by a high-pass characteristic, implying that cerebral autoregulation attenuates the effects of ABP changes on CBFV below 0.1 Hz. The presence of low-frequency peaks implies that CBFV may resonate in response to narrowband variations in ABP occurring at specific low frequencies, mitigating the aforementioned high-pass effect at specific low-frequency bands. The latter were found to vary with time and may be the result of nonstationary modulation of the cerebrovascular impedance by the autonomic nervous system and other factors, such as endothelial or metabolic mechanisms. The averaged first-order kernels over 20 successive 6 min segments for five different subjects are shown in Fig. 7, along with standard deviation bounds.

The second-order kernel (describing the nonlinear dynamics of the system) is shown in Fig. 8 for the same data segment, along with its corresponding frequency-domain representation (defined as the magnitude of the two-dimensional FFT of the second-order kernel). The frequency-domain peaks of the latter (symmetric about the diagonal) are related to the corresponding first-order frequency response peaks (for this specific segment) at 0.025 and 0.2 Hz. Note that the off-diagonal peak at (0.025, 0.2 Hz) implies nonlinear intermodulatory interactions between the mechanisms residing at the respective frequencies, whereas the diagonal peak at (0.025, 0.025 Hz) implies nonlinearity of the single mechanism residing at 0.025 Hz. Secondary peaks are discernible at the off-diagonal bi-frequency point (0.012, 0.05 Hz) and

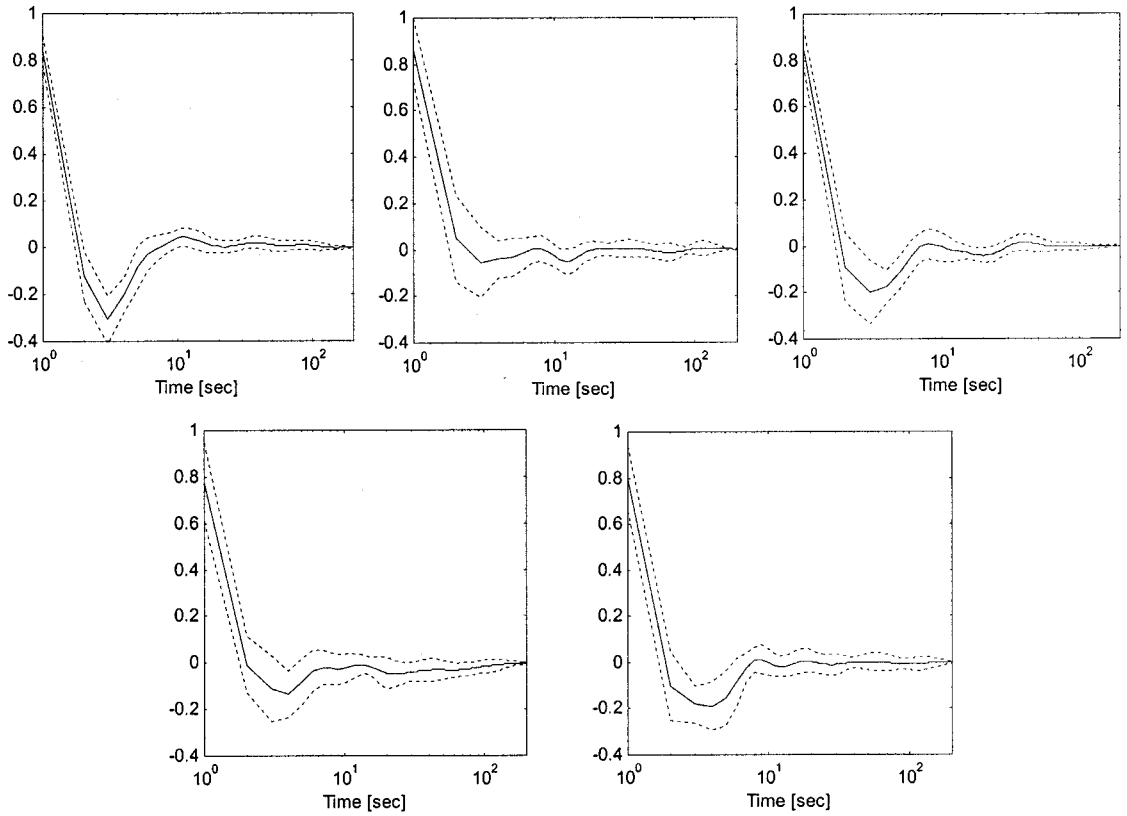

FIGURE 7. Average first-order kernels over 20 successive 6 min segments for five different subjects (solid lines) and corresponding standard deviation (dashed lines).

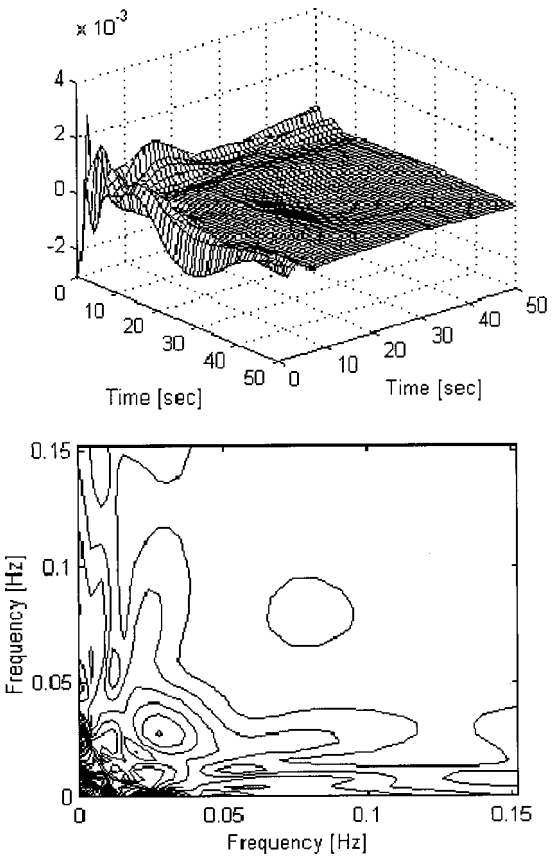

FIGURE 8. The second-order kernel for the data of Fig. 3. Upper panel: time domain, lower panel: frequency domain.

at the diagonal point (0.075, 0.075 Hz), both bearing an intriguing relation to the primary peak at 0.025 Hz (half, double and triple harmonic of 0.025 Hz).

Note that the location of the low and midfrequency (<0.1 Hz) peaks varies over time but stays within certain bounded neighborhoods from segment to segment (e.g., the 0.025 Hz peak stays within the 0.01–0.04 Hz neighborhood). The nonstationarity of the system dynamics (i.e., the varying locations of the spectral peaks and their respective strengths) can be tracked over time by estimating the system kernels for successive overlapping data segments. This is illustrated is Fig. 9 for the first-order kernels, where the first-order frequency responses evaluated from sliding 6 min windows with 4 min overlap are shown for two subjects over 2 h of data. The nonstationarity is evident, especially in low frequencies, but with no apparent pattern. However, reduced values of the FFT magnitude are consistently observed over time between 0.01 and 0.1 Hz.

To quantify the nonstationarity of the second-order kernel, eigen decomposition is performed and the first two eigenvalues are found to represent more than 95% of the kernel power. Therefore, the corresponding two eigenvectors define the significant nonlinear modes of the system and are tracked through time in the same manner as the first-order kernels (i.e., 6 min sliding data segments with 4 min overlap). Illustrative results are shown in the frequency domain in Fig. 10 for the two modes (multiplied with the respective eigenvalues) of the two subjects shown in Fig. 9. It is evident that the second-order (nonlinear) dynamics are more variable with time (nonstationary) than the first-order (linear) dy-

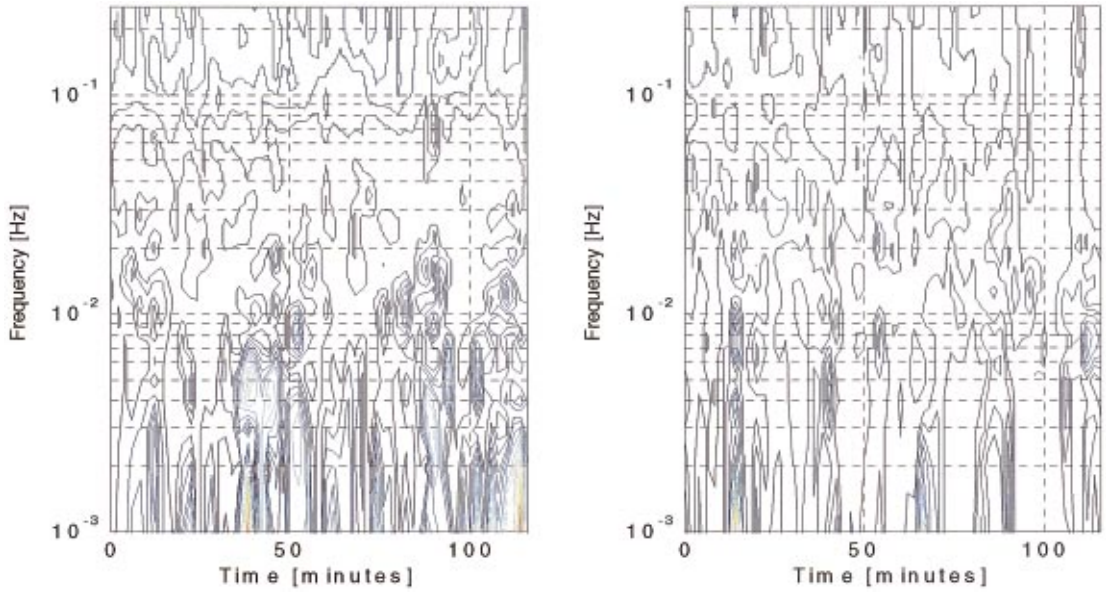

FIGURE 9. The first-order frequency response functions tracked over 2 h of data (6 min sliding data segments with 4 min overlap) for two subjects. The nonstationarity is evident and has random appearance.

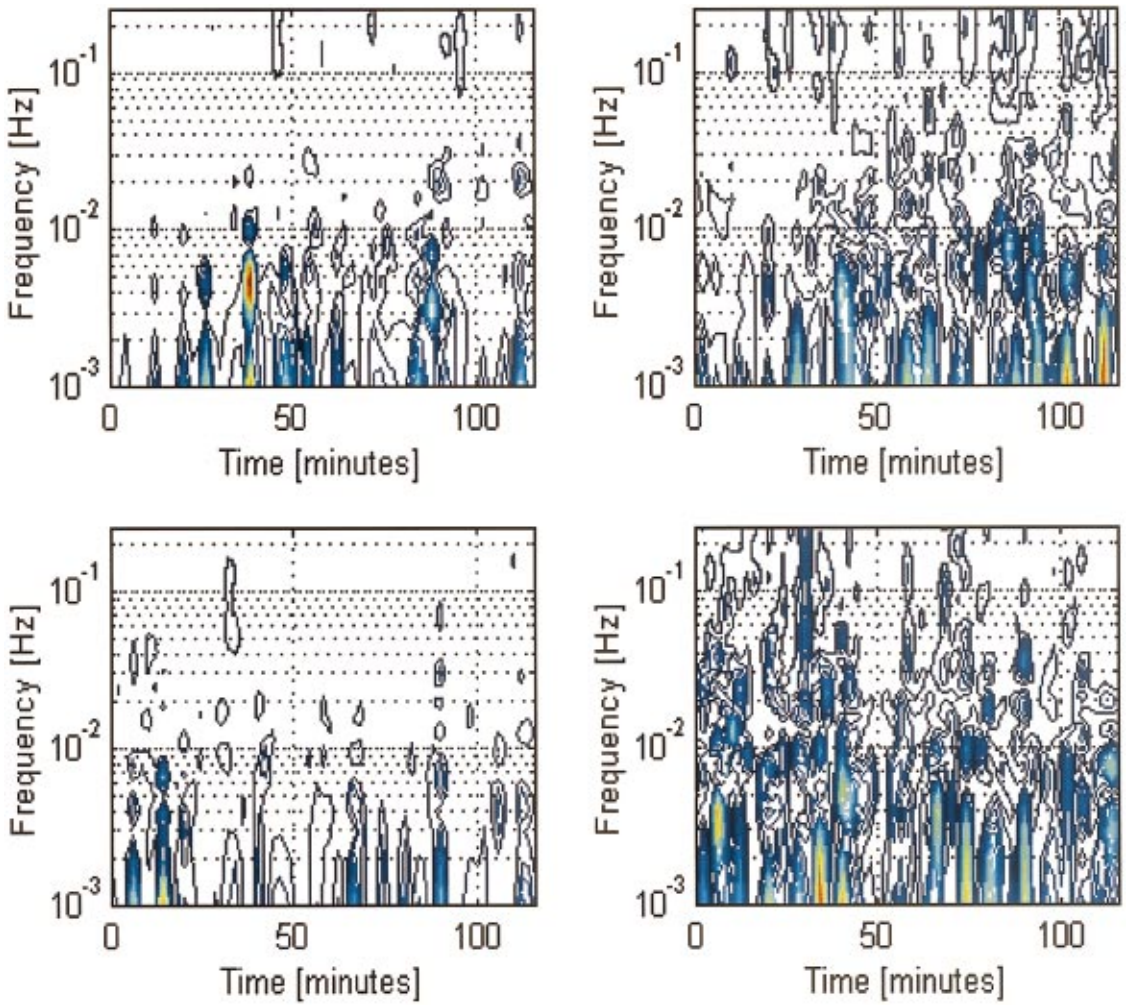

FIGURE 10. Time-frequency plots of the two significant modes of the second-order kernel for two different subjects, calculated from overlapping 6 min segments with a 4 min overlap (total of around 60 segments). Left panels: first mode, right panels: second mode.

namics, especially in the low and middle frequencies (<0.1 Hz). We also note that the second nonlinear mode is more nonstationary than the first mode and exhibits more peaks in the midfrequency range (0.01–0.1 Hz). Unlike the first-order kernel, the second-order kernel modes do not exhibit significant power in high frequencies (>0.1 Hz).

Although the study of nonstationarity deserves more future attention, a first attempt for quantification is the computation of a "variability index" over time for the kernel power at each discrete frequency bin f_i. If $p_j(f_i)$ denotes the power at the jth data segment at f_i, defined by the FFT magnitude of the kernel, then the variability index can be defined as

$$I(f_i)=\left\{\frac{1}{N-1}\sum_{j=1}^{N}[p_j(f_i)-\overline{p}(f_i)]^2\right\}^{1/2} \Big/ \overline{p}(f_i), \tag{10}$$

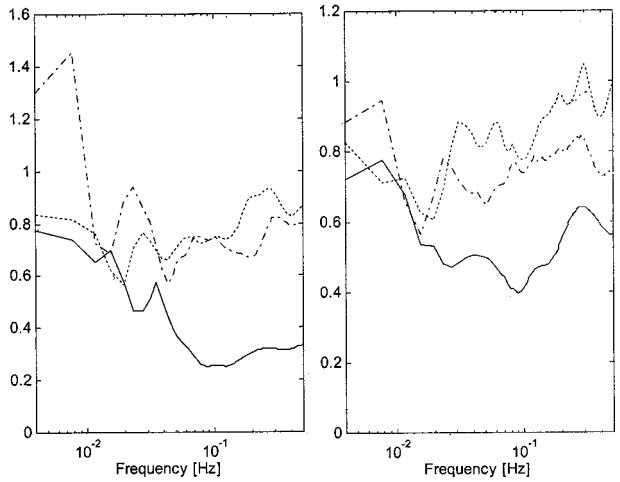

FIGURE 11. Variability indices for the two subjects of Figs. 9 and 10. Solid line: first-order kernel, dashed line: first mode of second-order kernel, dotted line: second mode of second-order kernel.

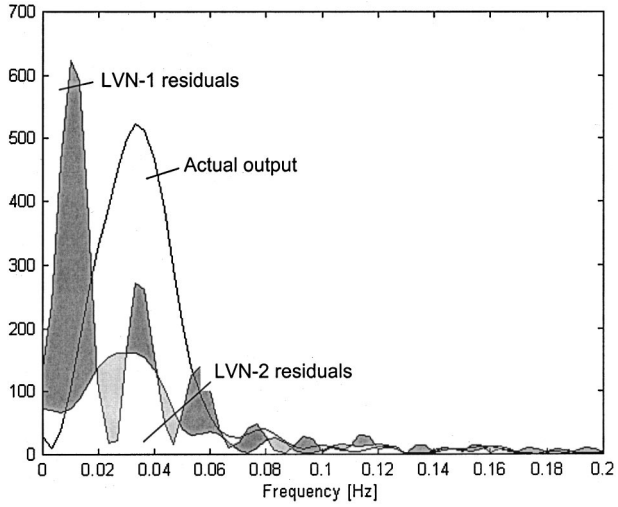

FIGURE 12. Output spectrum and spectra of output prediction residuals for LVN models with one (LVN-1) and two (LVN-2) filter banks for a testing data segment. The improved performance of the LVN-2 model is demonstrated by the preponderance of the dark shaded areas over the light shaded areas.

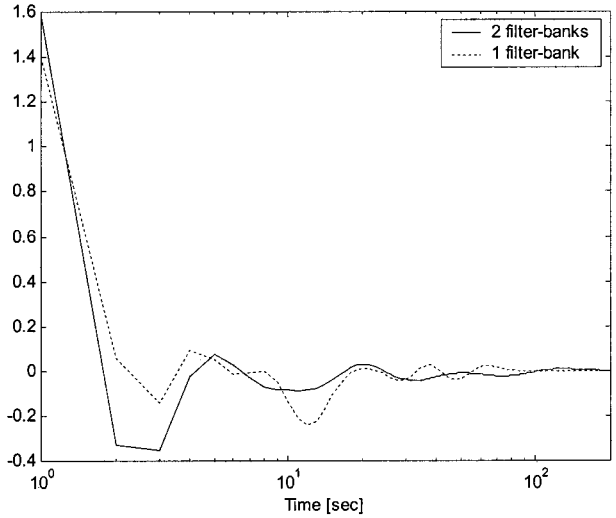

FIGURE 13. First-order kernels obtained from LVN models with one (LVN-1) and two (LVN-2) filter banks. The shape of the LVN-2 kernel is more consistent from segment to segment and yields lower prediction errors for the testing data segments.

where N is the number of segments and $\overline{p}(f_i)$ is the average of $p_j(f_i)$ over j for each frequency f_i. The computed variability indices for the first-order kernels and the second-order kernel modes are shown in Fig. 11 for the two subjects of Figs. 9 and 10.

Increased variability is observed in the low frequencies attributable to metabolic factors and in the middle frequencies, attributable to autonomic activity. Minimum variability is observed at frequencies above 0.12 Hz. The variability is evidently greater for the nonlinear dynamics.

We conclude this section with an illustration of the relative performance of the proposed method with two filter banks (LVN-2) versus the single filter-bank method (LVN-1). If we keep the number of free parameters the same for both methods ($L = 15$ for the LVN-1), the corresponding prediction errors for the testing data segments increase considerably (about 20% on the average) for the LVN-1, although the prediction errors for the training data segments are comparable. This can be seen in the spectra of the output residuals for a testing data segment (Fig. 12). The dark-shaded area indicates the frequency ranges where the performance of the LVN-2 exceeds that of the LVN-1, whereas the light-shaded area indicates the ranges where the reverse happens. It is clear that the overall performance of the LVN-2 is better, which is also reflected in the achieved NMSE (42.32% vs 56.66% in the LVN-1 case). This improvement is more evident below 0.02 Hz and above 0.05 Hz, demonstrating that the use of two filter banks (i.e., two distinct Laguerre parameters) captures better the two distinct time scales of the system dynamics. The first-order kernels are shown in Fig. 13 obtained from the two methods. The wave form of the kernel is more consistent from segment to segment for the LVN-2.

CONCLUSIONS

The presented results demonstrated the efficacy of the proposed approach in modeling nonlinear physiological systems with fast and slow dynamics, such as the autoregulation of cerebral hemodynamics. The slow dynamics were reliably estimated in the first-order (linear) and second-order (nonlinear) kernels, indicating that cerebral autoregulation has a longer memory (i.e., duration of causal effects from ABP changes to CBFV changes) than previously thought. Specifically, CBFV is affected by changes in ABP occurring up to a couple of minutes into the past—contrary to the prevailing view that the effects last only for a few seconds. The reliable estimation of the slow dynamics was not possible with previously used techniques and has become possible with the novel methodology introduced in the companion paper.[12] Since considerable ABP and CBFV signal power resides in the low-frequency range, the role of slow dynamics (i.e., low-frequency characteristics) is important for cerebral autoregulation. Thus, the advent of this new method offers a unique tool enabling proper analysis of cerebral autoregulation over the entire frequency range of interest.

The nonlinear characteristics of autoregulation were confirmed by comparing the prediction NMSEs achieved by linear and nonlinear models. The prediction NMSE was reduced by almost 20% when second-order (nonlinear) terms were included in the model, showing clearly

that the second-order nonlinear dynamics cannot be ne glected. Analysis of the spectral content of the first and second-order model residuals (output prediction errors) demonstrated that the nonlinearities reside primarily in the low and middle frequency range (below 0.1 Hz, and mostly below 0.04 Hz), a finding that agrees with previous studies based on coherence function measurements.[21]

The first-order (linear) dynamics of autoregulation were shown to have a fast differentiating component and a slow integrating/resonating component. The former responds to fast changes in ABP (above 0.1 Hz) and is responsible for the high-pass characteristic of autoregulation observed previously,[15,21] whereby changes in CBFV induced by ABP changes below 0.1 Hz are strongly attenuated. The observed negative undershoot of the first-order kernel (between 1 and 5 s) can be related to the cerebrovascular compliance and may have important clinical implications in the diagnosis and treatment of hypertension. On the other hand, the slow component exhibits peaks in the low (below 0.01 Hz) and mid (0.01–0.1 Hz) frequency ranges. The precise location of the peaks in the midfrequency range varies from segment to segment, exhibiting nonstationary behavior illustrated in Fig. 9 for two subjects over 2 h of data. Nonstationary behavior is also evident in the second-order nonlinear dynamics (described by the two significant modes of the second-order kernel) as illustrated in Fig. 10 for the same data. The nonlinear dynamics reside below 0.1 Hz and mostly below 0.04 Hz, as demonstrated by the spectra of the output prediction residuals shown in Fig. 4. Nonlinear interactions are identified by the off-diagonal peaks in the frequency domain representation of the second-order kernel, as illustrated in Fig. 8. The nonlinear dynamics exhibit greater variability over time (nonstationarity) than the linear dynamics, as illustrated in Figs. 9–11.

It is observed that the first nonlinear mode (derived from eigen decomposition of the second-order kernel) exhibits most of its power below 0.04 Hz and is less nonstationary than the second nonlinear mode, which also exhibits considerable power above 0.04 Hz and up to about 0.1 Hz. It is hypothesized that the nonlinear autoregulation mechanisms involve intermodulation effects of neural, metabolic, and endothelial factors on the impedance of the cerebrovascular bed in response to ABP changes.[7,16] In the higher frequency range (above 0.1 Hz), the regulatory mechanisms become less effective in attenuating CBFV changes in response to ABP changes, and the nonlinearities are absent.

Since the observed nonstationary behavior of the low-frequency peaks may be attributable to unobservable variables, such as metabolic activity, future studies will apply the presented methodology to the case of multi-input systems, whereby observable variables such as end-tidal CO_2 (surrogate for arterial CO_2) will be used as additional inputs[14] in order to quantify their combined dynamic effect (along with ABP changes) on CBFV fluctuations.

In conclusion, the improved accuracy achieved by nonlinear modeling methods can lead to a better quantitative understanding of dynamic cerebral autoregulation, in normal or pathophysiological cases (e.g., hypertension), under the influence of multiple systemic variables (neural and humoral) that have been long thought to have an effect but have not been amenable to quantification, due to intrinsic nonlinearities and nonstationarities. This may be potentially useful for clinical diagnosis of patients with cerebrovascular diseases.

ACKNOWLEDGMENTS

This work was supported by Grant No. RR-01861 awarded to the Biomedical Simulations Resource at the University of Southern California from the National Center for Research Resources of the National Institutes of Health and Grant No. 98BG058 awarded to the Institute for Exercise and Environmental Medicine, University of Texas Southwestern Medical Center at Dallas and Presbyterian Hospital of Dallas from American Heart Association Texas Affiliate.

REFERENCES

[1] Aaslid, R. K., W. Lindengaard, W. Sorterberg, and H. Nornes. Cerebral autoregulation dynamics in humans. *Stroke* 20:45–52, 1989.

[2] Chon, K. H., Y. M. Chen, N. H. Holstein-Rathlou, and V. Z. Marmarelis. Nonlinear system analysis of renal autoregulation in normotensive and hypertensive rats. *IEEE Trans. Biomed. Eng.* 45:342–353, 1998.

[3] Chon, K. H., Y. M. Chen, V. Z. Marmarelis, D. J. Marsh, and N. H. Holstein-Rathlou. Detection of interactions between myogenic and TGF mechanisms using nonlinear analysis. *Am. J. Physiol.* 267:F160–F173, 1994.

[4] Diehl, R. R., D. Linden, D. Lucke, and P. Berlit. Phase relationship between cerebral blood flow velocity and blood pressure. A clinical test of autoregulation. *Stroke* 26:1801–1804, 1995.

[5] Faraci, F. M., and D. D. Heistad. Regulation of the cerebral circulation: Role of endothelium and potassium channels. *Physiol. Rev.* 78:53–97, 1998.

[6] Giller, C. A. The frequency-dependent behavior of cerebral autoregulation. *Neurosurgery* 27:362–368, 1990.

[7] Heistad, D. D., and H. A. Kontos. Cerebral circulation. In: Handbook of Physiology. The Cardiovascular System. Peripheral Circulation and Organ Blood Flow. Bethesda, MD: Am. Physiol. Soc., 1983, Sec. 2, Vol. III, Part 1, Chap. 5, pp. 137–182.

[8] Kuo, T. B. J., C. M. Chern, W. Y. Sheng, W. J. Wong, and H. H. Hu. Frequency domain analysis of cerebral blood flow velocity and its correlation with arterial blood pressure. *J. Cereb. Blood Flow Metab.* 18:311–318, 1998.

[9] Lee, Y. W. and M. Schetzen. Measurement of the Wiener

kernels of a nonlinear system by cross-correlation. *Int. J. Control* 2:237–254, 1965.
[10] Marmarelis, V. Z. Identification of nonlinear biological systems using Laguerre expansions of kernels. *Ann. Biomed. Eng.* 21:573–589, 1993.
[11] Marsh, D. J., J. L. Osborn, and W. J. Cowley. 1/*f* fluctuations in arterial pressure and regulation of renal blood flow in dogs. *Am. J. Physiol.* 258:F1394–F1400, 1990.
[12] Mitsis, G. D., and V. Z. Marmarelis. Modeling of nonlinear systems with fast and slow dynamics. Methodology. *Ann. Biomed. Eng.* 30:272–281, 2002.
[13] Panerai, R. B., A. W. R. Kelsall, J. M. Rennie, and D. H. Evans. Frequency-domain analysis of cerebral autoregulation from spontaneous fluctuations in arterial blood pressure. *Med. Biol. Eng. Comput.* 36:315–322, 1998.
[14] Panerai, R. B., D. M. Simpson, S. T. Deverson, P. Mahony, P. Hayes, and D. H. Evans. Multivariate dynamic analysis of cerebral blood flow regulation in humans. *IEEE Trans. Biomed. Eng.* 47:419–423, 2000.
[15] Panerai, R. B., S. L. Dawson, and J. F. Potter. Linear and nonlinear analysis of human dynamic cerebral autoregulation. *Am. J. Physiol.* 277:H1089–H1099, 1999.
[16] Paulson, O. B., B. Strandgaard, and L. Edvinsson. Cerebral autoregulation. *Cerebrovasc. Brain Metab. Rev.* 2:161–192, 1990.
[17] Rissanen, J. Information Theory and Neural Nets. In: Mathematical Perspectives on Neural Networks, edited by P. Smolensky, M. C. Mozer, and D. E. Rumelhart. Mahwah, NJ: Lawrence Erlbaum Associates, 1996, pp. 567–602.
[18] Tiecks, F. P., A. M. Lam, B. F. Matta, S. Strebel, C. Douville, and D. W. Newell. Effects of the Valsalva maneuver on cerebral circulation in healthy adults. A transcranial Doppler study. *Stroke* 26:1386–1392, 1995.
[19] Tiecks, F. P., A. M. Lam, R. Aaslid, and D. W. Newell. Comparison of static and dynamic cerebral autoregulation measurements. *Stroke* 26:1014–1019, 1995.
[20] Zhang, R., J. H. Zuckerman, and B. D. Levine. Spontaneous fluctuations in cerebral blood flow velocity: Insights from extended duration recordings in humans. *Am. J. Physiol.* 278:H1848–H1855, 2000.
[21] Zhang, R., J. H. Zuckerman, C. A. Giller, and B. D. Levine. Transfer function analysis of dynamic cerebral autoregulation in humans. *Am. J. Physiol.* 274:H233–H241, 1998.